

OPEN ACCESS

Characteristics of gain degradation in proton irradiated Low Gain Avalanche Detectors

To cite this article: T. Ceponis et al 2025 JINST 20 C08029

View the article online for updates and enhancements.

You may also like

- Ghosts in irradiated trench isolated LGADs G. Laštovika-Medin, G. Kramberger, J. Kroll et al.
- Achieving near 100% Fill factor for small pixel LGADs: Study of First Trench Isolated LGADs fabricated at Micron Semiconductor Ltd Fasih Zareef, Neil Moffat, Richard Bates et
- Feasibility study of a proton CT system based on 4D-tracking and residual energy determination via time-of-flight Felix Ulrich-Pur, Thomas Bergauer, Alexander Burker et al.





RECEIVED: May 13, 2025 REVISED: July 31, 2025 ACCEPTED: August 12, 2025 PUBLISHED: August 29, 2025

20th Anniversary Trento Workshop on Advanced Silicon Radiation Detectors Trento, Italy 4–6 February 2025

Characteristics of gain degradation in proton irradiated Low Gain Avalanche Detectors

T. Ceponis[®],* M. Biveinyte, L. Deveikis[®], E. Gaubas[®], J. Pavlov[®], V. Rumbauskas[®], V. Tamosiunas[®] and K. Zilinskas

Institute of Photonics and Nanotechnology, Vilnius University, Sauletekio ave. 3, LT-10257, Vilnius, Lithuania

E-mail: tomas.ceponis@ff.vu.lt

ABSTRACT. Low Gain Avalanche Detectors (LGADs) provide high time resolution at moderate charge gain, making them essential for high-energy physics experiments, such as those at the High Luminosity Large Hadron Collider. However, their performance is significantly impacted by radiation induced defects, particularly at high hadron fluences. This study is devoted to the characterization of degradation mechanisms in LGADs irradiated with 24 GeV/c protons at fluences ranging from 10^{12} to 10^{16} cm⁻². Carrier lifetime (τ_R) variations examined using the microwave probed photoconductivity transients revealed a significant reduction of τ_R from >10 μ s in non-irradiated samples to <1 ns at the highest fluence irradiated sensors, indicating increased densities of defects acting as deep-level recombination centers. Photoionization and deep level transient spectroscopy techniques have been employed to identify radiation induced defects. The impact of these defects on the electric field distribution and internal gain in LGADs was comprehensively analyzed using Synopsys TCAD Sentaurus and MATLAB simulations. The results indicate a substantial reduction in gain from 26 for non-irradiated sensors to a negligible its value for 10^{16} cm⁻² fluence irradiated LGADs due to a simultaneous reduction of effective doping concentration, decreased τ_R and enhanced trapping. The study provides a versatile methodology for correlating electrical and spectroscopic measurements with defect characterization, offering valuable insights for optimizing LGAD design in radiation-rich environments.

Keywords: Charge transport and multiplication in solid media; Radiation damage to detector materials (solid state); Radiation-hard detectors; Particle tracking detectors (Solid-state detectors)

^{*}Corresponding author.

| Contents |
|----------|
|----------|

| 1 | Intr | 1 | | | |
|---|-------------------------------------|--|---|--|--|
| 2 | Samples and experimental techniques | | | | |
| | 2.1 | Samples | 2 | | |
| | 2.2 | Experimental techniques | 2 | | |
| 3 | Exa | mined characteristics | 3 | | |
| | 3.1 | Variations of electric properties | 3 | | |
| | 3.2 | Recombination characteristics in LGADs | 4 | | |
| | 3.3 | DLTS and PIS spectra recorded in LGADs | 5 | | |
| | 3.4 | Characteristics of internal gain | 8 | | |
| 4 | Sun | nmary | 9 | | |

1 Introduction

Low Gain Avalanche Detectors (LGADs) comprise a class of silicon-based sensors that combine high temporal resolution with moderate charge gain, making them valuable for high-energy physics (HEP) applications [1]. LGADs are particularly suitable for 4D tracking in collider experiments, such as those in the High Luminosity Large Hadron Collider (HL-LHC), where precise timing information is crucial for mitigating pile-up effects [2, 3]. The internal gain mechanism of LGADs, which can reach up to 100, contributes to their superior timing capabilities [1]. LGADs provide a significant improvement in time resolution due to their internal gain, which enhances the signal-to-noise ratio and enables measurements with precision at few tens of picoseconds level [4]. This capability is particularly beneficial for particle tracking in HEP experiments, where precise time resolution is essential for distinguishing closely spaced events. The decrease of LGAD gain with irradiation due to acceptor removal in the multiplication layer [5] is a key problem leading to a limitation of LGAD functionality. This acceptor removal in p-type silicon appears due to radiation caused formation of B_iO_i defect complexes [6] owing to Watkins boron replacement mechanism [7]. The reduction of effective doping might also appear due to compensation of effective acceptors by holes trapped at the energy levels in the band-gap [5]. The partially activated boron mechanism can be an additional explanation of the acceptor removal in LGADs [5, 8, 9]. However, the latter mechanism is rather complicated and depends on temperature processing history, including the formation of iron-boron pairs and transformations of other defects [10, 11]. Additionally, carrier recombination lifetime (τ_R) is strongly dependent on the irradiation fluence [12], with a dramatic decrease of τ_R at high fluences, potentially contributing to reduced charge collection efficiency. Therefore, a correlative study of the variations of electrical and radiation defect characteristics is necessary to identify the key factors responsible for the degradation of sensor performance. Actually, the estimation of the B_iO_i concentration within the gain layer of irradiated LGADs using standard techniques, such as deep level transient spectroscopy, is complicated due to full depletion of the active region and capacitance

drop to the geometrical value. In this work, we present a comprehensive study of the degradation of 24 GeV/c proton-irradiated LGADs by combining the electrical and spectral characterization of sensors with the incorporation of various simulation tools, such as Synopsys TCAD Sentaurus.

2 Samples and experimental techniques

2.1 Samples

In this work, the p-type Si sensors of $n^{++}p^+pp^{++}$ (*LGAD* — Low Gain Avalanche Detector) structure, produced by Hamamatsu Photonics (HPK) company, were investigated. The sensor structures, the same as those presented in figure 1 for ref. [13], consisted of a 150 µm low resistivity (p^{++}) support wafer, a 50 µm active p-type layer, and a highly-doped n^{++} cathode region. The width of the n^{++} region was approximately 1 µm, where the doping concentration was in the range of 10^{18} – 10^{19} cm⁻³. Additionally, the sensors had an implanted highly-doped p⁺ multiplication layer with a dopant concentration of ~ 3×10^{16} cm⁻³. The anode and cathode electrodes were metalized with aluminium, and a square non-metalized window of 100×100 µm² area was formed within the cathode for optical carrier injection. A gold bump was deposited on the cathode Al layer for better electrical contact. A guard ring was formed at the cathode to increase the breakdown voltage. Samples were irradiated at CERN with 24 GeV/c relativistic protons with fluences (Φ) ranging from 10^{12} to 10^{16} protons/cm² with ~ 10^{11} protons per spill. The detector chips comprised arrays of 2×2 sensors, while the active area of a single sensor was 1.3×1.3 mm².

2.2 Experimental techniques

Measurements of current-voltage (I-V) and capacitance-voltage (C-V) characteristics were performed using a Summit 11000B-AP probe station equipped with Keysight Technologies E4980A LRC meter and a Keysight Technologies B2912B Source/Measure Unit (SMU).

A commercial system produced by "Particulars, Advanced Measurement Systems" company was employed to measure injected charge drift current transients and evaluate collected charge and gain of sensors. The bias voltage was varied using an external source-measure-unit Keithley 2410. The signals were recorded using a 2.5 GHz Lecroy WR9254 oscilloscope. The measurements of the injected charge drift currents were performed at room temperature in dark.

Carrier recombination lifetime was measured by employing the 22 GHz microwave probed photoconductivity (MW-PC) transient technique [12]. Excess carriers were generated by an STA-01 microchip YAG:Nd laser with a 400 ps pulse duration at a wavelength of 1064 nm focused to a spot of $<50\,\mu m$ width and positioned within LGAD layer. Samples were positioned vertically relative to the microwave antenna to probe signals from the sample polished edge of the LGAD structure.

Deep-level transient spectroscopy (DLTS) measurements were conducted using a commercial HERA-DLTS 1030 system (PhysTech GmbH) with Fourier-transform-based spectral averaging [14]. Majority and minority carrier trap spectra were recorded at a reverse bias voltage (U_R) of -25 V, to preserve control of the gain layer thickness under varied measurement regimes. The 1 s pulses of $U_P = -5$ V and $U_P = 2$ V were employed for filling the majority and minority carrier traps, respectively. These parameters were selected based on the analysis of the C-V characteristics and the effective doping profile to probe the gain layer of the sensor. The Laplace transform method

was employed for high-resolution analysis of overlapping spectral peaks. The measurements were conducted over a temperature range of 40–300 K.

The quasi-steady-state photoionization spectroscopy (PIS) was employed for spectroscopy of radiation induced defects at elevated irradiation fluences. The LGAD photo-current changes were recorded under device edge illumination by the 800 W photometric lamp, with spectral variations dispersed using a DMR-4 double-prism monochromator, and under applied reverse voltage of -20 V capable of depleting the gain layer. Samples were placed in a liquid nitrogen cryostat with a VIS-IR transparent entrance window, and the temperature was maintained at 78 K during measurements. The PI spectrum exhibited multiple spectral steps, associated with a definite trap with photo-activation energy E_{PIS} . The PIS signal is dependent on the incident photon energy hv due to variation of the photon-electron interaction cross-section $\sigma(hv)$, which determines the shape and position of PIS spectral steps [15].

3 Examined characteristics

3.1 Variations of electric properties

The measured I-V and C-V characteristics are illustrated in figures 1(a) and 1(b), respectively. It can be seen that the leakage current increases with irradiation fluence. Additionally, a step of the current increase in the I-V characteristics is observed at reverse voltages ranging from 30 V to 50 V, and it shifts to the low voltages with the increase of irradiation fluence. This step is related to the full depletion of the gain layer, followed by the full depletion of the low doped active volume of the sensors. At higher voltages (>140 V), a steep increase in leakage current is observed, which is related to the breakdown in the p^+ layer of LGADs.

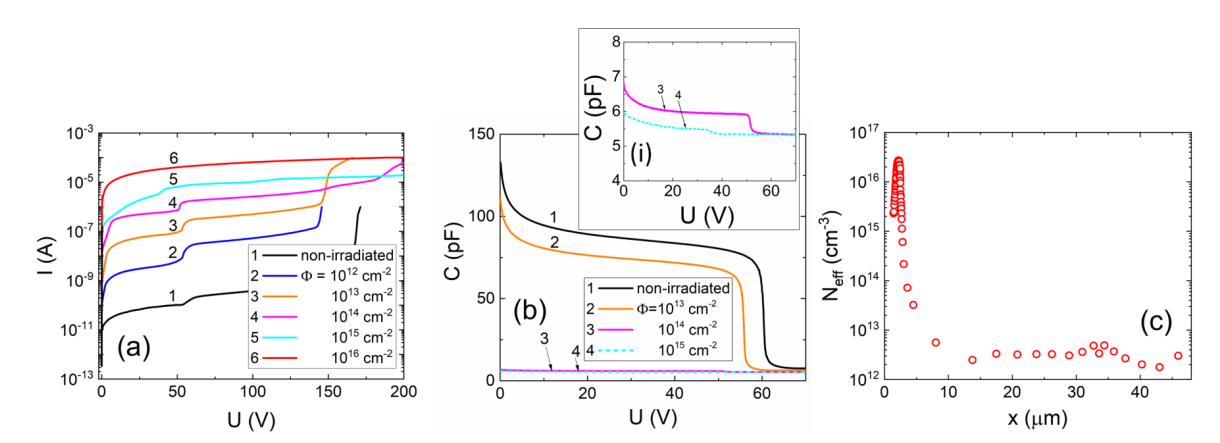


Figure 1. I-V (a) and C-V (b) characteristics measured in LGADs irradiated with different proton fluences. (c) – The estimated effective doping profile in the non-irradiated sensor. In the inset (i) for figure (b), the C-V characteristics for LGADs irradiated with proton fluences $\Phi \ge 10^{14}$ cm⁻² are enlarged to highlight the depletion voltage of the gain layer.

C-V characteristic measured at 1 MHz frequency in a non-irradiated sensor is characterized by a hyperbolic decrease of barrier capacitance in the reverse voltage range of <60 V due to depletion of the gain layer (p^+) and a sudden decrease of capacitance at higher voltage values due to depletion of the low-doped active volume (p) of the sensor. The effective doping density N_{eff} can be easily

evaluated from C-V characteristic using the relation $N_{\rm eff}w = -C^3/(q\varepsilon\varepsilon_0 S^2({\rm d}C/{\rm d}U_R))$, with w – the depletion width, ε – the dielectric permittivity, ε_0 – the vacuum permittivity, q – the elementary charge, S – the area of the junction. The calculated $N_{\rm eff}$ profile in non-irradiated LGAD is presented in figure 1(c), and the gain layer width of 1–2 µm can be extracted, which is in line with evaluations obtained for the same technology devices [16]. The character of the C-V changes correlates with the I-V characteristics, indicating (in the inset (i) for figure 1(b)) the reduction of gain layer depletion voltage with the increase of irradiation fluence. The barrier capacitance decreases with enhancement of irradiation fluence (figure 1(b)), and at the highest irradiation fluences the barrier capacitance approaches the geometrical value: $C_{\rm geom} = \varepsilon\varepsilon_0 S/d$, where d is the width of the active region. This result hints on the reduction of the effective doping density $N_{\rm eff}$ within the gain layer of LGADs.

3.2 Recombination characteristics in LGADs

Carrier recombination lifetime is directly related to the functional performance of the sensors. The MW-PC transients recorded in pristine and in proton irradiated LGADs are presented in the inset (i) of figure 2. These MW-PC transients in the irradiated Si materials exhibit a single-exponential decay with the relaxation rate increasing with irradiation fluence. Therefore, the effective carrier lifetime ($\tau_{\rm eff}$) is determined from the carrier concentration (n) reduction related to the linear decay using the recorded photoconductivity relaxation transients and is given by $\tau_{\rm eff} = n/(-\partial n/\partial t)|_{\rm exp(-1)}$. The effective carrier lifetime was corrected to estimate the bulk lifetime ($\tau_b = \tau_R$) using the relation $\tau_b^{-1} = \tau_{\rm eff}^{-1} - \tau_s^{-1}$, where τ_s accounts for surface recombination effects [11, 12, 17–19]. Value of τ_s is estimated either from simulations including parameters of layer thickness and carrier diffusion coefficient or analysis of photoconductivity relaxation variations dependent on excitation wavelength [12]. As shown in figure 2, the τ_R is inversely proportional to the irradiation fluence and the estimated τ_R decreases from >10 μ s in the non-irradiated sensors to <1 ns in 10¹⁶ cm⁻² fluence irradiated sensors. This strong degradation in lifetime is attributed to the increased density of radiation-induced defects that act as deep-level recombination centers within the silicon material, contributing to the reduced charge collection efficiency of LGADs.

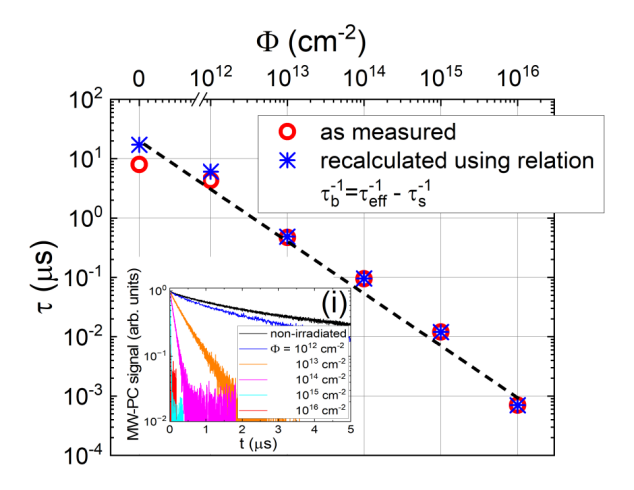


Figure 2. The as-measured and recalculated bulk recombination lifetime values as a function of proton irradiation fluence. In the inset (i) MW-PC transients recorded in different proton fluences irradiated LGADs.

3.3 DLTS and PIS spectra recorded in LGADs

To identify the radiation-induced defects responsible for the degradation of sensor performance, deep-level transient spectroscopy (DLTS) was employed for sensors irradiated with $\leq 10^{12}$ cm⁻² proton fluences. The recorded spectra of majority carrier traps and minority carrier traps are presented in figures 3(a) and 3(b), respectively.

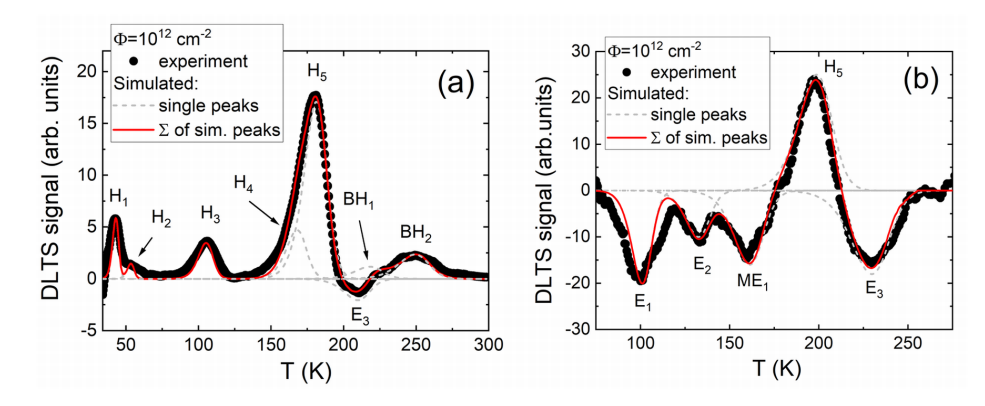


Figure 3. DLTS spectra of the majority (a) and minority (b) carrier traps recorded on LGADs irradiated with 10^{12} cm⁻² proton fluence.

To improve the resolution of overlapping peaks, the correlation function and Laplace transform techniques were applied for analysis of the recorded DLTS spectra. Subsequently, these spectra were simulated using the DLTS Phystech software [14]. The simulations involved iterative adjustments of trap parameters, such as carrier activation energy and capture cross-section, to match the calculated and experimental DLTS spectra. This approach enabled the accurate estimation of the dominant trap parameters. The identification of traps was done by comparison of experimentally obtained trap signatures with those reported in literature.

Up to seven peaks (labelled H) associated with majority carrier traps were identified in the DLTS spectra (figure 3(a)). The trap H_1 , with an activation energy of 0.078 eV, is attributed to the double interstitial-oxygen complex (I_2O) [20]. H_2 , with an activation energy of 0.105 eV, is associated with a triple vacancy (V_3) [20]. H_3 , with activation energy of 0.186 eV, is attributed to a complex of double and triple vacancy (V_2+V_3) [20]. The doublet consisting of traps H_4 and H_5 , with activation energies of 0.362 eV and 0.373 eV, respectively, is assigned to carbon-oxygen complexes — H₄ corresponding to the metastable (CO*) and H_5 to the stable (CO) configuration [20]. Finally, the traps BH_1 and BH_2 , with activation energies of 0.440 eV and 0.530 eV, respectively, are attributed to different configurations of the divalent bistable defect (DBH) [21]. In DLTS spectra, four peaks related to minority carrier traps (labelled E) were identified, as shown in figure 3(b). The trap E_1 , with an activation energy of 0.159 eV, is associated with the vacancy-oxygen (VO) complex [22]. E2, with an activation energy of 0.227 eV, is attributed to the interstitial boron-interstitial oxygen complex $(B_i O_i)$, which plays a key role in acceptor removal in the p-type silicon [22]. The metastable defect ME₁, with an activation energy of 0.272 eV, is another configuration of the above-mentioned DBH defect [21]. The trap E₃, with an activation energy of 0.420 eV, is associated with a vacancy cluster (V_{cl}) [22]. Key parameters of these traps, including activation energy E_T , capture cross-section σ , concentrations, and defect identification, are summarized in table 1. Unfortunately, DLTS spectroscopy could not be applied to sensors irradiated at fluences $\geq 10^{13}$ cm⁻² due to radiation defect concentration exceeding dopant density.

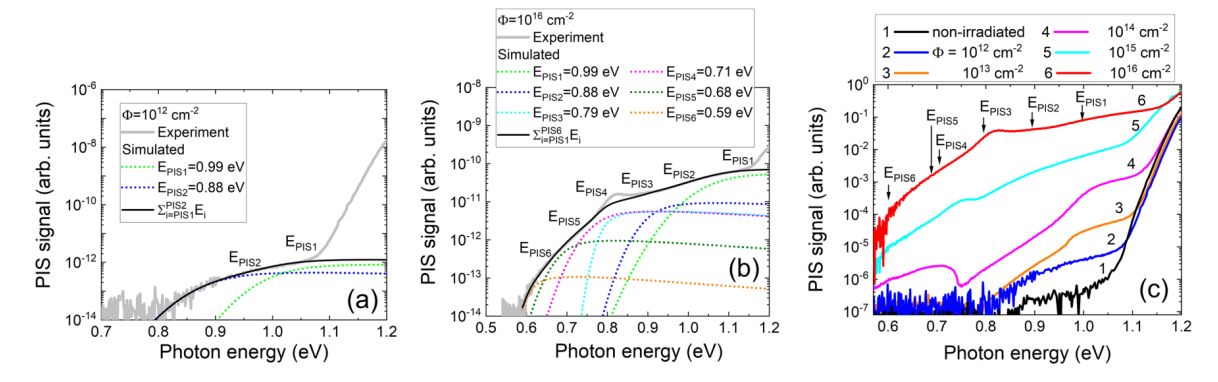


Figure 4. PIS spectra in the proton irradiated LGADs with fluences of 10^{12} cm⁻² (a) and 10^{16} cm⁻² (b). The dotted lines correspond to the simulated spectral steps using the Kopylov-Pikhtin model [15], while solid black lines represent the sum of all spectral steps. (c) – Comparison of PIS spectra measured in LGADs irradiated with different fluences. The spectra are normalized to the peak current value.

Table 1. The parameters of majority and minority carrier traps revealed in LGADs irradiated with the 24 GeV/c protons of fluence 10^{12} cm⁻². The traps and their photo-ionization energies estimated by PIS in LGADs irradiated in the 10^{12} – 10^{16} cm⁻² range of fluences are also listed.

| DLTS | | | | | | PIS | | |
|------------------|---------------------|-----------------------------------|--|-------------------------------------|-------------------|-----------------------|-------------------------------------|--|
| Trap | E _T (eV) | $\sigma \times 10^{-16}$ (cm^2) | $N_{\rm T} \times 10^{12}$ (cm^{-3}) | Defect [Ref.] | Trap | E _{PIS} (eV) | Defect [Ref.] | |
| H_1 | 0.078 | 23.6 | 0.17 | I ₂ O [20] | | | | |
| H_2 | 0.105 | 90 | 0.41 | V ₃ [20] | | | | |
| $\overline{H_3}$ | 0.186 | 3.8 | 1.03 | V ₂ +V ₃ [20] | E _{PIS1} | 0.99 | V ₂ +V ₃ [20] | |
| $\overline{H_4}$ | 0.362 | 83.2 | 1.36 | $C_i O_i^* [20]$ | | | | |
| H ₅ | 0.373 | 23 | 48.8 | C_iO_i [20] | E _{PIS3} | 0.79 | C_iO_i [24] | |
| BH_1 | 0.440 | 9.9 | 0.35 | DBH [21] | E _{PIS4} | 0.71 | DBH [21] | |
| BH_2 | 0.530 | 27.1 | 0.66 | DBH [21] | | | | |
| E_1 | 0.159 | 2.7 | 5.60 | VO [22] | | | | |
| E_2 | 0.227 | 7.8 | 2.89 | B_iO_i [22] | E _{PIS2} | 0.88 | B_iO_i [23] | |
| ME_1 | 0.272 | 3.9 | 4.46 | DBH [21] | | | | |
| $\overline{E_3}$ | 0.440 | 27.1 | 5.11 | V _{cl} [22] | E _{PIS4} | 0.71 | V _{cl} [22] | |
| | | | | | E _{PIS5} | 0.68 | V ₂ O [24, 25] | |
| | | | | | E _{PIS6} | 0.59 | I-center/cluster [25] | |

The PIS spectroscopy was employed for the characterization of sensors irradiated with fluences $\geq 10^{13}$ cm⁻². Generation of the excess carriers directly depends on the photo-ionization cross-section σ . Thereby, measurements of spectral dependence of the photocurrent induced by excess carriers enable evaluation of the activation energy of photo-active centers. The PIS signal mainly originates from the depleted region of the sensor controlled by the applied reverse voltage. The carriers are excited within the entire volume of the sensors; however, the contribution of excess carriers photo-excited in the neutral region is negligible within the PIS response. In this work, the measurements were implemented at a reverse voltage of -20 V, therefore, only the gain layer of the sensor was partially

depleted. Thereby, only the traps within the gain layer are controlled by PIS. However, reduction of the effective doping concentration under elevated irradiation fluences and consequent extension of the depletion region might lead to some inaccuracies in the quantitative estimation of trap parameters. From two to six spectral steps could be distinguished within PI spectra measured in LGADs irradiated with fluences in the 10^{12} – 10^{16} cm⁻² range (figure 4). However, it is impossible to unambiguously clarify whether the PI step is determined by electron or hole transitions. Therefore, in this study, the attribution of the PI spectral peaks to specific defects was performed by combining the literature data and the obtained DLTS results. The activation energy values have been estimated using the Kopylov- Pikhtin [15] model. The extracted parameters obtained by simulating these PIS peaks are summarized in table 1. Thereby, the spectral peak $E_{PIS1} = 0.99 \, eV$ can be associated with a complex of double and triple vacancies (V_2+V_3) [20]. $E_{PIS2} = 0.88 \, eV$ is attributed to B_iO_i [23] defect.

 $E_{PIS4} = 0.79 \,\text{eV}$ can be assigned to $C_i O_i$ [24] complex. The peak $E_{PIS4} = 0.71 \text{ eV}$ could be associated with the divalent bistable defect (DBH) [21], as can be deduced from DLTS analysis. Therefore, it might be both the hole or electron trap. As an electron capture center, it can be related to the vacancy cluster V_{cl} [22]. The $E_{PIS5} = 0.68 \,\text{eV}$ peak can be assigned to divacancy-oxygen complex V₂O [24, 25], while $E_{PIS6} = 0.59 \,\text{eV}$ was identified as the I-center or cluster [25] defect. The certain trap species listed in table 1, particularly V_2+V_3 , B_iO_i , C_iO_i and V_{cl} , have been identified using both DLTS and PIS techniques. The amplitude of the PI spectral step also depends on the filling of a deep trap, for instance, emptying of the filled center appears in the case of electron capture and thereby the PIS process depends on the trap and excess carrier concentration. This factor can be employed for the rough quantitative evaluation of radiation in-

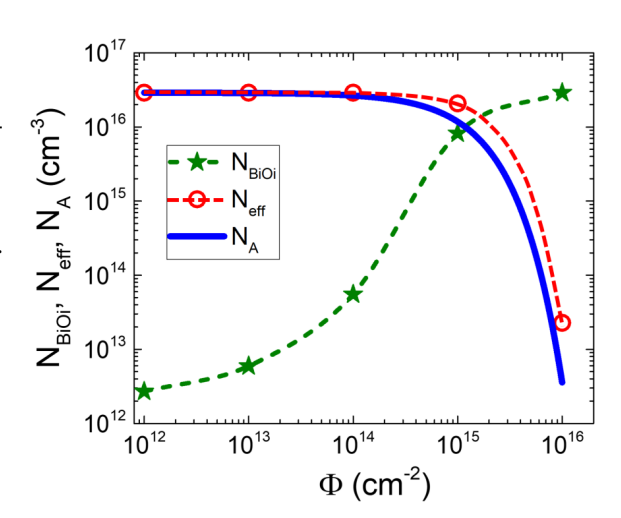


Figure 5. Variations of experimentally obtained $N_{\rm BiOi}$ and $N_{\rm eff}$ as a function of proton irradiation fluence compared with the acceptor concentration N_A calculated using the widely employed parametrization model for acceptor removal in p-type Si [6] with acceptor removal constant $c_A = 9 \times 10^{-16} \, {\rm cm}^2$.

duced defect type. The variation of concentration of the B_iO_i (N_{BiOi}) complexes under the impact of irradiation is of the main interest since the reduction of gain in LGADs is mainly caused by the acceptor removal due to the formation of the B_iO_i complexes. For the sample irradiated with 10^{12} cm⁻² fluence, the amplitude of the E_{PIS2} spectral peak can be associated with the same N_{BiOi} center, characterized using DLTS. Then, the relative variations of the amplitude of the E_{PIS2} (figure 4(c)) as a function of irradiation fluence represent the changes of N_{BiOi} concentration. These N_{BiOi} variations, together with the estimated $N_{eff}(\Phi)$ within the gain layer as $N_{eff}(\Phi) = N_{eff}(0) - N_{BiOi}(\Phi)$, are displayed in figure 5 as a function of irradiation fluence. These experimentally obtained $N_{eff}(\Phi)$ are in line (figure 5) with the widely employed parametrization model for acceptor removal in p-type Si [6], as $N_A(\Phi) = N_{A,0} \exp(-c_A\Phi)$, with $c_A = 9 \times 10^{-16}$ cm² being the acceptor removal constant. The value of the c_A was taken from ref. [6] for $N_{eff}(0) = 3 \times 10^{16}$ cm⁻³. However, as mentioned above, at higher irradiation fluences, the depletion region might extend to the active layer of the sensors, leading to

~20% inaccuracies in evaluating the absolute values of $N_{\rm eff}(\Phi)$ and $N_{\rm BiOi}(\Phi)$. These inaccuracies might also appear due to compensation of effective acceptors by holes trapped at the defect levels in the band-gap [5] and partially activated boron mechanism [5, 8, 9] as mentioned above.

3.4 Characteristics of internal gain

Measurements of the internal gain were performed by the TCT technique recording the induced charge drift current transients. The internal gain of the LGADs was estimated as the ratio between the collected charge (time-integrated current pulse) in the LGAD and the TCT collected charge within the pin diode structure (identical to the LGAD structure without the gain layer). This ratio of collected charges has been examined under the same measurement conditions (temperature, laser intensity) [26]. The internal gain of the LGADs was measured at carrier injection of less than 10 MIPs. The gain increases from 8 at $U_R = 60 \text{ V}$ to 26 at $U_R = 160 \text{ V}$ for the non-irradiated LGAD, as shown in figure 6(a), and no degradation is observed for the low fluence ($\leq 10^{13}$ cm⁻²) irradiated samples. At higher fluences, the gain decreases and approaches a negligible value at the highest fluence of $\Phi = 10^{16} \, \text{cm}^{-2}$. In order to reveal the mechanisms responsible for the gain degradation, the simulations have been performed using the following conditions and steps: i) the simulation of the distribution of the electric field was done using Synopsys TCAD Sentaurus software and employing the experimentally obtained N_{eff} profile (figures 1(c) and 5), ii) the gain was simulated in Matlab platform using the previously obtained electric field distribution and employing the methodology described in ref. [27]. Our simulation results (figure 6(b)) provide an additional link between the experimental results presented in figure 5 and figure 6(a). A modest reduction of N_{eff} to approximately 96.5 % of the initial value $N_{\rm eff0}$ indeed can lead to an observed nearly halving of the gain at $\Phi = 10^{14} \, \rm cm^{-2}$ at a given voltage, while $N_{\rm eff}$ drop to half of the initial value fully eliminates the gain. The negligible gain at irradiation fluence $\Phi = 10^{16} \, \text{cm}^{-2}$ can additionally be explained by the reduction of τ_R (figure 1) and/or trapping time to < 1 ns, when it becomes shorter than the carrier drift time represented by the pulse duration (2–3 ns) of the current transient, leading to a reduction of drifting carriers. Therefore, the presented methodology is well-suited for the comprehensive characterization of the LGAD characteristics under the impact of irradiation.

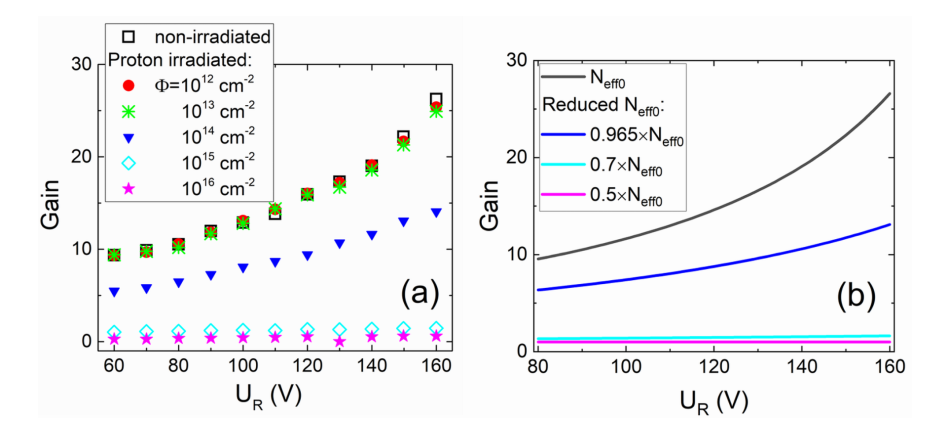


Figure 6. Variations of measured (a) and simulated (b) internal gain characteristics of LGADs as a function of reverse voltage for different irradiation fluences (a) or $N_{\rm eff}$ (b).

4 Summary

The characteristics of the radiation caused degradation in Low Gain Avalanche Detectors (LGADs) irradiated with 24 GeV/c protons at fluences ranging from 10^{12} to 10^{16} cm⁻² show that significant reduction of τ_R from >10 µs in non-irradiated LGADs to <1 ns for the highest fluence irradiated sensors, due to increased densities of deep-level recombination centers lead to reduction of multiplication factor in processes of impact ionization. Deep level transient spectroscopy (DLTS) and photoionization spectroscopy (PIS) enabled the identification of the dominant radiation defects listed in table 1. The characteristics of the specific defects and their role in the electric field distribution and internal gain degradation have been related by employing Synopsys TCAD Sentaurus and MATLAB simulations. It has been demonstrated that the internal gain decreased from 26 for non-irradiated sensors to a negligible value for 10^{16} cm⁻² fluence irradiated LGADs due to the reduction of effective doping concentration and decreased τ_R and enhanced trapping. It has been demonstrated that the employed comprehensive methodology for assessing the impact of irradiation on LGAD performance, emphasizing the importance of defect identification and lifetime analysis, is rather suitable for optimizing the LGAD-type radiation sensor design.

Acknowledgments

This project has received funding from the Research Council of Lithuania (LMTLT), agreement No. S-CERN-24-6. Roberta Arcidiacono is acknowledged for providing the samples for investigation. The sample irradiations were performed in the framework of the European Union's Horizon Europe Research and Innovation programme under Grant Agreement No. 101057511.

References

- [1] G. Giacomini, W. Chen, G. D'Amen and A. Tricoli, *Fabrication and performance of AC-coupled LGADs*, 2019 *JINST* 14 P09004 [arXiv:1906.11542].
- [2] S. Ali et al., Performance in beam tests of carbon-enriched irradiated Low Gain Avalanche Detectors for the ATLAS High Granularity Timing Detector, 2023 JINST 18 P05005 [arXiv:2303.07728].
- [3] X. Zhang et al., One-Dimensional Position-Sensitive LGAD With a DC Coupled and Resistive Charge Division Mechanism, IEEE Trans. Nucl. Sci. 70 (2023) 853.
- [4] E. Currás, M. Fernández and M. Moll, *Gain reduction mechanism observed in Low Gain Avalanche Diodes*, *Nucl. Instrum. Meth. A* **1031** (2022) 166530 [arXiv:2107.10022].
- [5] G. Kramberger et al., *Radiation effects in Low Gain Avalanche Detectors after hadron irradiations*, 2015 *JINST* **10** P07006.
- [6] M. Moll, Acceptor removal Displacement damage effects involving the shallow acceptor doping of p-type silicon devices, PoS Vertex2019 (2020) 027.
- [7] G.D. Watkins, Intrinsic defects in silicon, Mater. Sci. Semicond. Process. 3 (2000) 227.
- [8] T.E. Seidel and A.U. Mac Rae, *The isothermal annealing of boron implanted silicon*, *Radiat. Eff.* **7** (1971) 1.
- [9] K. Hara et al., *Improvement of timing resolution and radiation tolerance for finely segmented AC-LGAD sensors*, presentation at the *18th "Trento" Workshop on Advanced Silicon Radiation Detectors*, Trento, Italy, 28 February–2 March 2023, https://indico.cern.ch/event/1223972/contributions/5262001/.

- [10] A. Kaniava et al., Recombination activity of iron-related complexes in silicon studied by temperature dependent carrier lifetime measurements, Appl. Phys. Lett. 67 (1995) 3930.
- [11] S. Rein, Lifetime Spectroscopy: A Method of Defect Characterization in Silicon for Photovoltaic Applications, Springer (2005) [DOI:10.1007/3-540-27922-9].
- [12] E. Gaubas, E. Simoen and J. Vanhellemont, Review Carrier Lifetime Spectroscopy for Defect Characterization in Semiconductor Materials and Devices, ECS J. Solid State Sci. Technol. 5 (2016) P3108.
- [13] X. Yang et al., Layout and performance of HPK prototype LGAD sensors for the High-Granularity Timing Detector, Nucl. Instrum. Meth. A 980 (2020) 164379 [arXiv:2003.14071].
- [14] PhysTech GmbH, *Product catalog*, http://www.phystech.de/products/dlts/dlts.htm [Accessed 08 May 2025].
- [15] A.A. Kopylov and A.N. Pikhtin, *Influence of temperature on spectra of optical absorption by deep levels in semiconductors*, Sov. Phys. Solid State **16** (1975) 1200.
- [16] X. Shi, Radiation Campaign of HPK Prototype LGAD sensors for the High-Granularity Timing Detector (HGTD), ATL-LARG-SLIDE-2019-903 (2019).
- [17] J.S. Blakemore, Semiconductor statistics, Pergamon Press (1962).
- [18] A. Rose, *Concepts in photoconductivity and allied problems*, Interscience Publishers John Wiley & Sons (1963).
- [19] S.M. Ryvkin, *Photoelectric effects in semiconductors*, Consultants Bureau (1964).
- [20] T. Ceponis et al., Study of radiation-induced defects in p-type $Si_{1-x}Ge_x$ diodes before and after annealing, Materials 13 (2020) 5684.
- [21] L.F. Makarenko et al., Formation of a Bistable Interstitial Complex in Irradiated p-Type Silicon, Phys. Status Solidi A 216 (2019) 1900354.
- [22] J. Pavlov et al., 5.5 MeV electron irradiation-induced transformation of minority carrier traps in p-type Si and $Si_{1-x}Ge_x$ alloys, Materials 15 (2022) 1861.
- [23] L.I. Khirunenko et al., *Electronic absorption of interstitial boron-related defects in silicon*, *Phys. Status Solidi A* **214** (2017) 1700245.
- [24] B.C. MacEvoy, G. Hall and K. Gill, *Defect evolution in irradiated silicon detector material*, *Nucl. Instrum. Meth. A* **374** (1996) 12.
- [25] E. Gaubas, A. Uleckas and J. Vaitkus, Spectroscopy of neutron irradiation induced deep levels in silicon by microwave probed photoconductivity transients, Nucl. Instrum. Meth. A 607 (2009) 92.
- [26] E. Currás Rivera, A. La Rosa, M. Moll and F. Zareef, Gain layer degradation study after neutron and proton irradiations in Low Gain Avalanche Diodes, 2023 JINST 18 P10020 [arXiv:2306.11760].
- [27] E. Currás Rivera and M. Moll, Study of Impact Ionization Coefficients in Silicon With Low Gain Avalanche Diodes, IEEE Trans. Electron. Dev. 70 (2023) 2919 [arXiv:2211.16543].